Instrument Science Report WFC3 2008-19

WFC3 TV2 Testing: IR Intrapixel sensitivity

P. McCullough
August 26, 2008

ABSTRACT

We derive an approximate intrapixel sensitivity variation (IPSV) of the IR-1 detector of WFC3 from ground-test imagery. The purpose was to assess whether additional testing of this sort should be performed in Thermal Vacuum 3 (TV3) testing, scheduled to commence in February 2008. Whereas NICMOS exhibits IPSV as large as 40%, peak to valley, in the photometry of stars observed in J band with the NIC3 detector (Lauer 1999), WFC3 IR is expected to show much smaller IPSV and the results reported here confirm that expectation, with IPSV less than 8% peak to valley, or 1.6% rms, for a PSF similar to that expected on orbit for WFC IR at ~1 micron. The results reported here are based upon data from a test that was not intended for the purpose of measuring IPSV and hence should be considered preliminary. Given the limited precision of the results reported here, we designed additional tests of IPSV and implemented them in TV3 on the flight detector (IR-4), results of which will be described in a subsequent report, WFC3 ISR 2008-29.

Introduction

The response of a pixilated detector to incident light may show variation in the detected charge integrated over the point-spread function (PSF) due to intrapixel sensitivity variation (IPSV). A lab test designed to study IPSV might illuminate the detector from a fiber optic cable, the tip of which can be much smaller than a pixel, and by raster scanning, one can map the IPSV with very fine sub-pixel precision. By an equivalent optical technique using a fast focal ratio to produce a sub-pixel-sized spot,

Barron et al. (2007) measured IPSV for a few 1.7-micron cutoff IR sensors. Barron report small IPSV, i.e. more uniform response, for sensors with high quantum efficiency (QE) and large IPSV for sensors with low quantum efficiency. Barron et al. also noted a surprising asymmetric IPSV for one (high QE) sensor. For flight detectors such as WFC3, especially only months before launch, such a lab test could delay the schedule, increase cost, and especially increase risk of damaging the detector. Also, any IPSV measured with a scanned fiber-optic technique must be transformed to the *effective* IPSV measured with the telescope and instrument's PSF. The technique used here illuminates the detector with a PSF and focal ratio similar to those expected on orbit, and hence is more directly relevant to an astronomer's needs, i.e. stellar photometry, than the scanned-fiber technique, which may be of greater interest to an engineer that designs detectors.

Data

During Thermal Vacuum test 2 (TV2) in the summer of 2007, we obtained three datasets in which a continuum (tungsten lamp + F128N filter in WFC3) point source was imaged hundreds of times as it drifted across the WFC3 detectors, in order to monitor image stability. The sequence of observations interleaved sets of IR-1 observations with sets of UVIS-2 observations, permitting us to monitor the brightness of the source with the UVIS-2 detector. The point source drifts across a few pixels over many hours, and that variation in position permits us to study IPSV. The data were obtained with the TVTEST "UV12S03 Image Stability" during 2-day-long runs, at three epochs over the course of 30 days (Figure 1). The IR observations were interleaved with the UVIS observations (Figure 2) in a pattern that repeats every 30 minutes, typically. All of the data analyzed here originated from the files stored in /grp/hst/wfc3/opusdata/ in subdirectories ir1/ and uvis2/ with file names of the form "iu12*flt.fits." Those images were flat-fielded with dummy flats, i.e. divided by unity, and were stored in the nominal HST format on or before Aug 3, 2007. We flat-fielded them by dividing by a single IR-1 flat field, "ii130b04r_07183063904_flt.fits" although doing so had only a small effect on the final results, specifically the IPSV with (and without flat-fielding) is 8% (11%) peak-to-valley and 1.6% (2.4%) r.m.s.). Flat fielding has no effect on our conclusions.

Analysis

A custom IDL script organizes the data and performs very simple aperture photometry of the point source in each image. The same script operates on the UVIS and IR data with only minor changes in the input parameters. The script extracts a subarray from the *flt.fits files at the nominal positions of the point source on the UVIS and IR detectors. It then identifies the first image in which the point source either disappears entirely or moves far away from its nominal position, and defines that as a "background" image, which is subtracted from all the subarrays that exhibit the point source. Because

the point-source flux is so large compared to the pattern noise in the "background" image, the selection of the particular image hardly matters; the purpose of background subtraction is to make zero counts correspond to zero flux from the point source. The script then identifies the brightest pixel in the background-subtracted (subarray) image and records six values associated with that image: the FITS file name, the X centroid, the Y centroid, the total counts within an aperture of radius=8 pixels, the X and Y positions of the brightest pixel, and the value (counts) in that pixel. Executing the script on the IR-1 data and the UVIS data in turn produces, respectively, 664 and 2211 lines of such filenames, centroids, and fluxes, which are plotted and interpreted here.

Discussion

Within any given epoch of the three epochs, the photometry measured with the IR detector varies much more than that measured with the UVIS detector (Figure 1). The random component of the measurement uncertainty, as evident from the sample-to-sample variation, is much smaller than the systematic errors evident as drifts in the photometry over time scales of hours. The IR and UVIS observations were interleaved (Figure 2), so we interpolate the UVIS observations in order to compare them with the IR observations. The trajectories of the point source on the detectors are similar in physical scale, after accounting for the relative sizes of the detector pixels, and similar in their shapes (Figures 3 and 4), so we conclude that the dominant cause of the image motion is common for the IR and UVIS channels and is optically prior to the channel select mechanism inside WFC3. The aperture photometry measured with the IR-1 and UVIS-2 detectors is illustrated in Figures 5 and 6 respectively, and Figure 7 shows the ratio of the two. The ratio of measured fluxes varies by 8% peak to valley, with noticeable trends, either in time or in location – we cannot distinguish between the two from these data, apparently.

Under the assumptions that 1) the temporal variations in flux are removed by interpolation of the UVIS-2 photometry, and 2) all pixels have similar IPSV, we can investigate whether the flux-ratio variation evident in Figure 7 is due to IPSV by shifting the pattern of Figure 7 into pixel phase using the modulo function on the (X,Y) centroids measured on the IR-1 sensor. The result is shown in Figure 8, but the 2-dimensional measurement of IPSV is indistinct. Any grouping of pixels of a common color may not be due to pixel phase (X mod 1, Y mod 1) but instead could be due to proximity in time or position on the IR-1 detector. That is, one or both of the two assumptions mentioned before may be invalid. For example, the dark blue points at lower left nearly all come from the middle of the first epoch (cf. Figure 1) at (X,Y) = (14.2,15.2) (cf. Figure 7). Another example: the yellow-and-orange string of points extending from slightly above the middle of Figure 8 to its upper-left come from the third epoch and X<13. Because we cannot definitively disentangle the contributions of pixel phase, time, and position, we

consider the characterization of the IPSV as preliminary and quantitatively unreliable, although we anticipate that the 1.6% rms and 8% peak to valley may represent upper limits, because additional contributions (incorrectly calibrated temporal or spatial variations) are more likely to increase variation than cancel it out.

Figure 9 verifies the convention that (X mod 1, Y mod 1) = (0.5,0.5) corresponds to the centers of pixels. As expected, the flux in the brightest pixel is highest in cases in which the core of the PSF is concentrated as much as possible into one pixel, i.e. the centroid is in the center of a pixel, lower toward the edges (the flux is split in two by the edge), and lowest near the corners (the flux is split amongst four adjacent pixels).

Conclusions

We recommend additional testing to either measure the IPSV of the WFC3 IR detector or to improve the upper limits given in the abstract. The experience documented here indicates that tests designed for long-term monitoring of image stability are generally inadequate for also measuring IPSV due to difficulty in maintaining or calibrating flux variations with time as compared to variations with respect to position on the sensor. A test designed to measure IPSV should be short in duration so that temporal variation in the flux incident upon the detector is negligible.

References

Barron, N. et al. 2007, Subpixel Response Measurement of Near-Infrared Detectors, PASP, 119, 466

Lauer, T. R. 1999, The Photometry of Undersampled Point-Spread Functions, PASP, 111, 1434

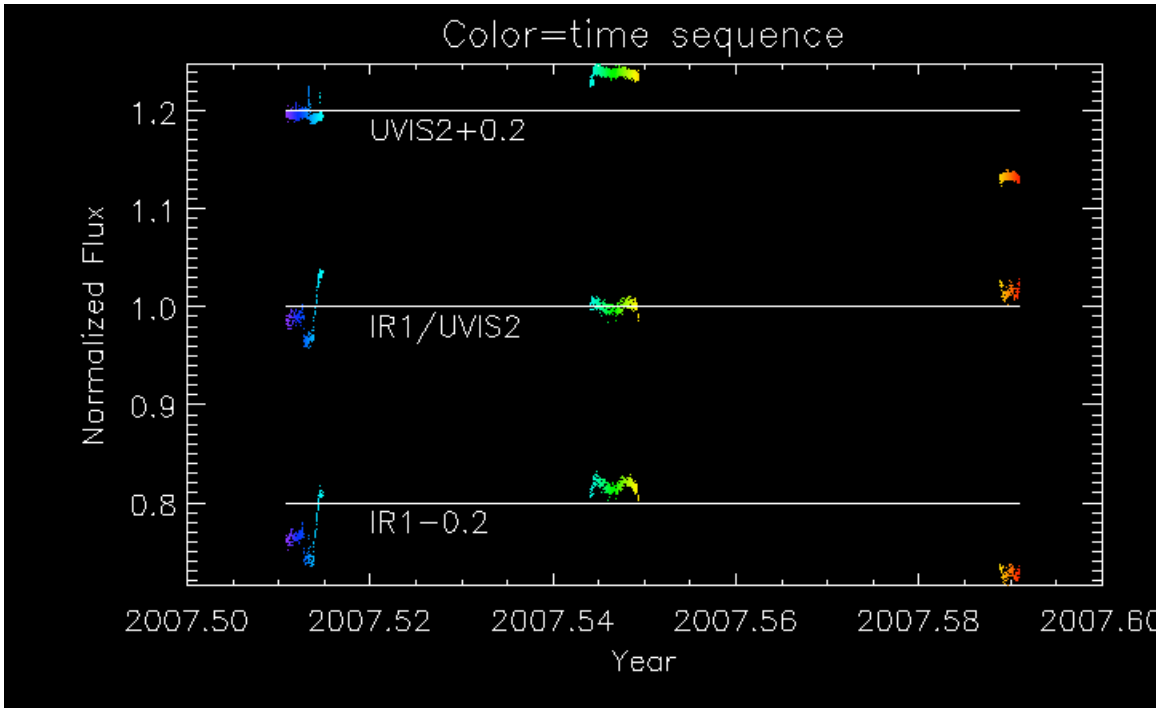

Figure 1: Flux versus time. This illustrates one of the color schemes used in subsequent plots: a rainbow color table ranges from the earliest (purple) to latest (red) observations analyzed. The flux in a photometric aperture, normalized separately to the median of UV and IR measurements, is plotted at top (UVIS), bottom (IR) and in the middle (the ratio, IR/UVIS); the three times series are shifted vertically by 0.2 for clarity. On short timescales, the IR photometry varies more than the UVIS photometry, although both detectors were observing the same source. For reasons unknown, the last epoch (2007.59) exhibits a larger IR/UVIS ratio than the first two epochs; whether that is due to lower flux on the UVIS detector or higher flux on the IR detector is unknown.

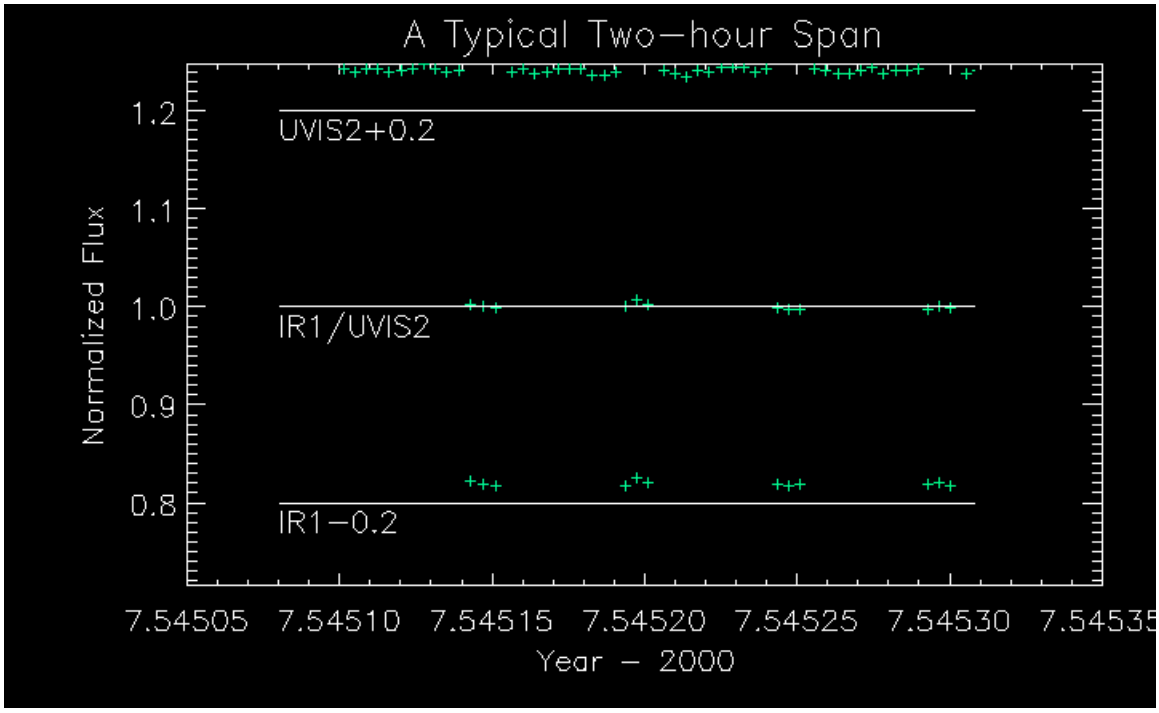

Figure 2: Same as Figure 1, but zoomed in to a two-hour span to show the interleaved sequence of UVIS and IR measurements.

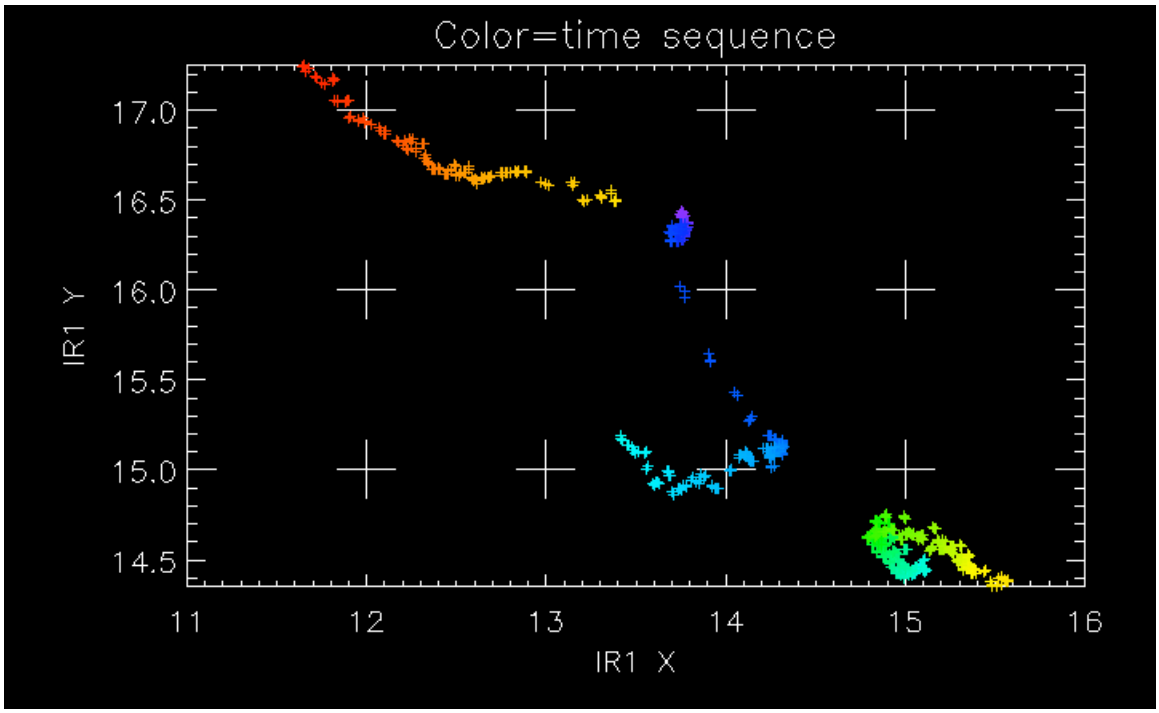

Figure 3: Trajectory of the point source's centroid on the WFC3 IR-1 detector. The corners of pixels are indicated by + symbols. Arbitrary offsets have been subtracted from X and from Y. In this diagram, color indicates time (cf. Figure 1). The position at the beginning of the first epoch of observation is (X,Y) = (13.7,16.4) and drifts to the lower right, then levels off at Y=15 and moves leftward to end at (X,Y) = (13.4,15.2). The second epoch of observations is the set of points near (X,Y)=(15,14.5) and the third epoch begins near (X,Y) = (13.5,16.5) and drifts to the upper-left.

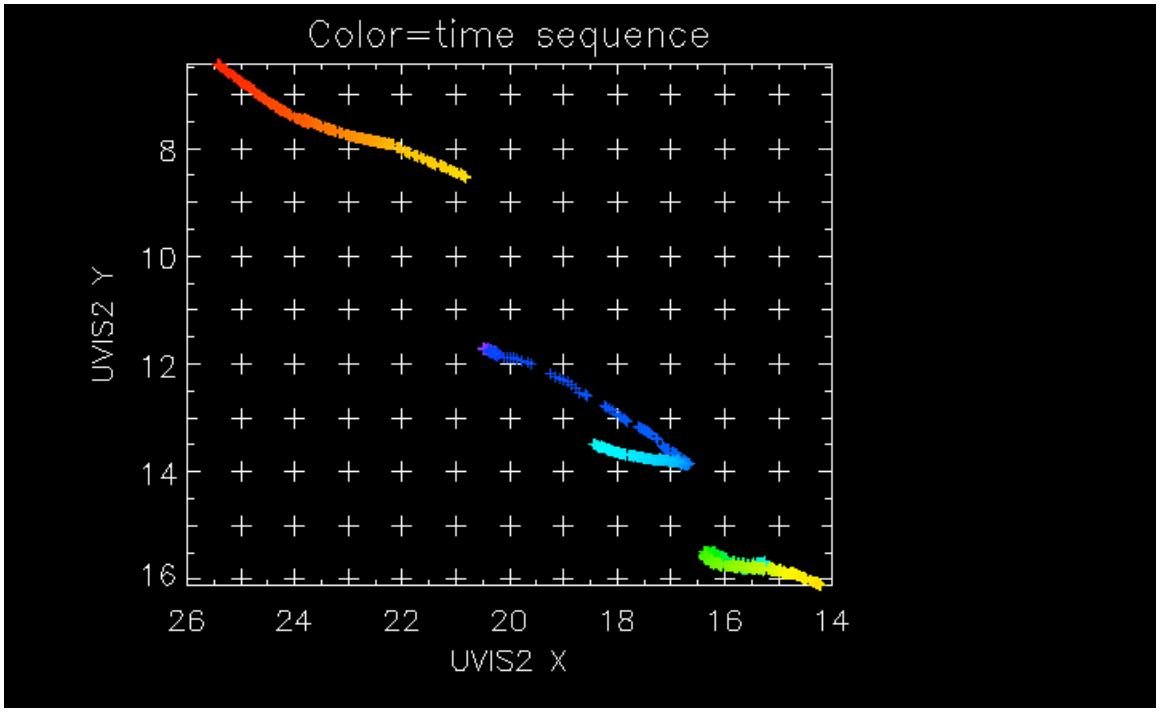

Figure 4: Same as Figure 3 but for the UVIS-2 detector. The (X,Y) coordinates have been re-oriented (flipped and rotated by a multiple of 90 degrees) to make the trajectory's pattern match that of Figure 3. Each UVIS-2 (and IR-1) pixel is approximately square of width 0.04 arcsec (0.13 arcsec for IR-1). The trajectories on the UVIS-2 and IR-1 detectors are nearly the same in angular units, suggesting that the main cause of the image motion is optically "prior to" the channel select mechanism.

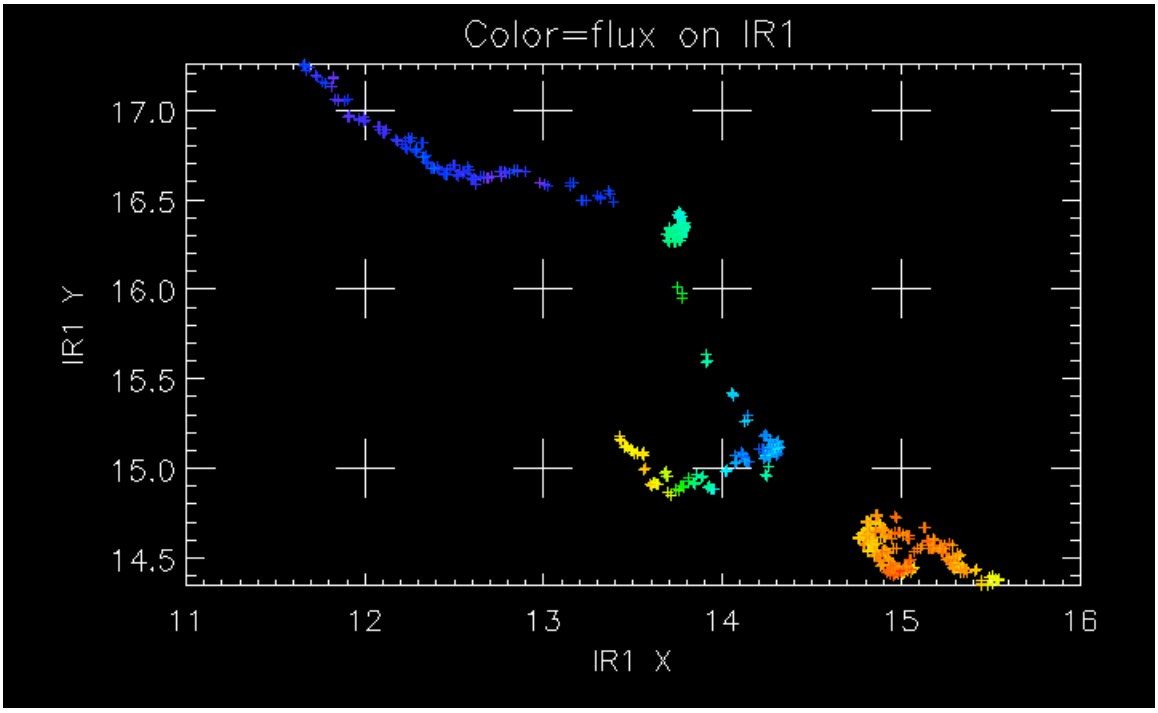

Figure 5: Same trajectory as Figure 3, except here color corresponds to the normalized flux on the IR-1 detector. In so far as the flux measured by the UVIS-2 detector is nearly constant during any given epoch (Figure 1), one may assume the incident flux on the IR-1 detector is also nearly constant during any given epoch. The changes in flux (in this diagram, color) during the last epoch (X < 13) could be interpreted as the anticipated variation with pixel phase: darker blue (lower ratio) at edges and corners, and lighter blue (larger ratio) at the center of the pixel centered on (X,Y) = (12.5,16.5). On the other hand, the middle epoch (X > 14.5) shows the opposite trend with pixel phase: orange (larger ratio) at the pixel edge and yellow (lower ratio) away from the edge to either side. Furthermore, the trend of first epoch (X~14) doesn't correlate with pixel phase and presumably has a cause different than IPSV.

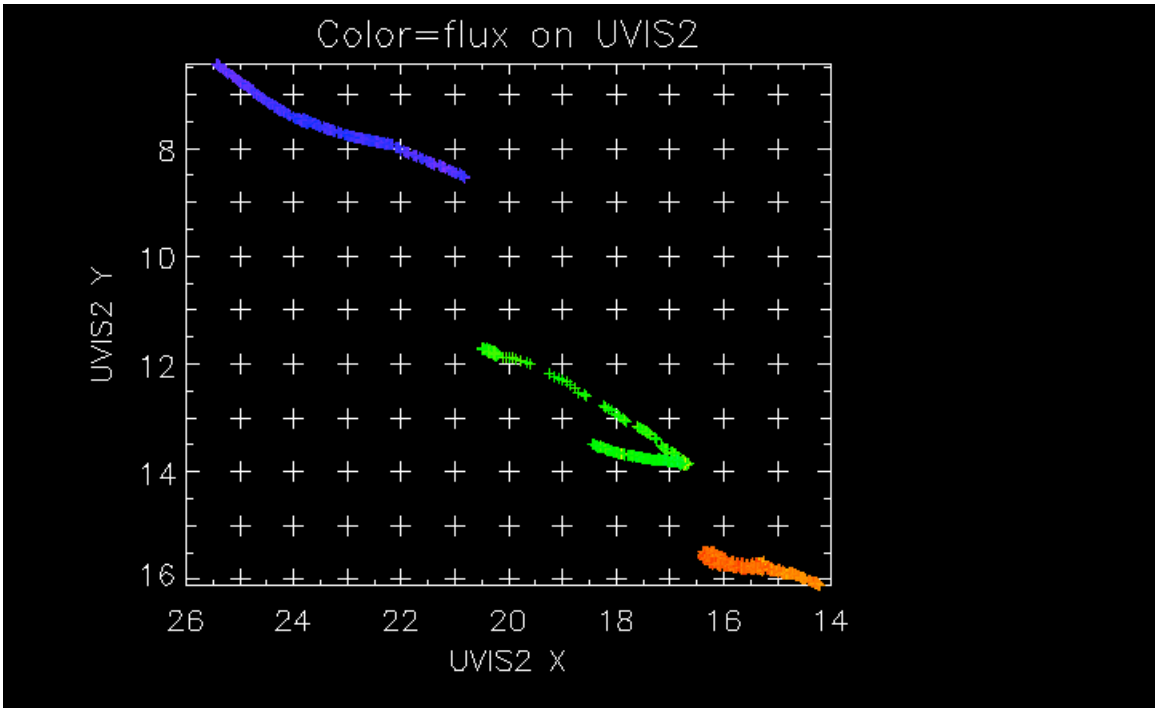

Figure 6: Same trajectory as Figure 4, except here color corresponds to the normalized flux on the UVIS-2 detector.

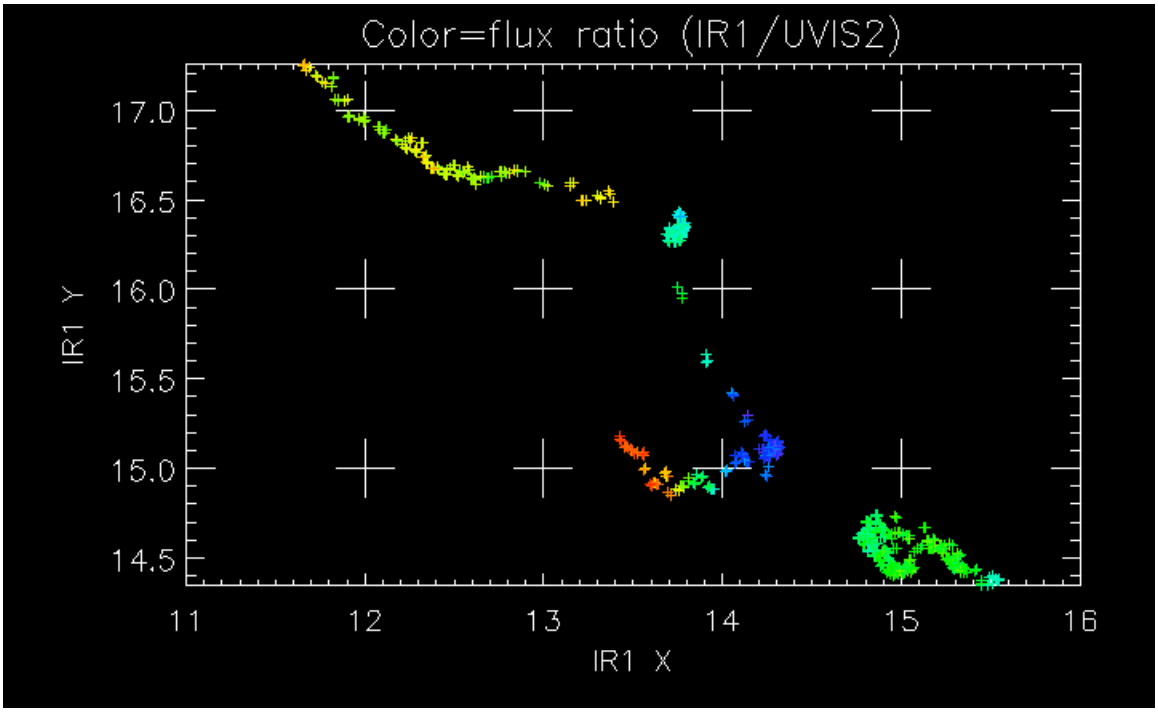

Figure 7: Same trajectory as Figure 3, except here color corresponds to the normalized flux ratio (IR-1 divided by UVIS-2) on the two detectors. The fluxes are integrated within synthetic circular apertures appropriate for each detector and PSF.

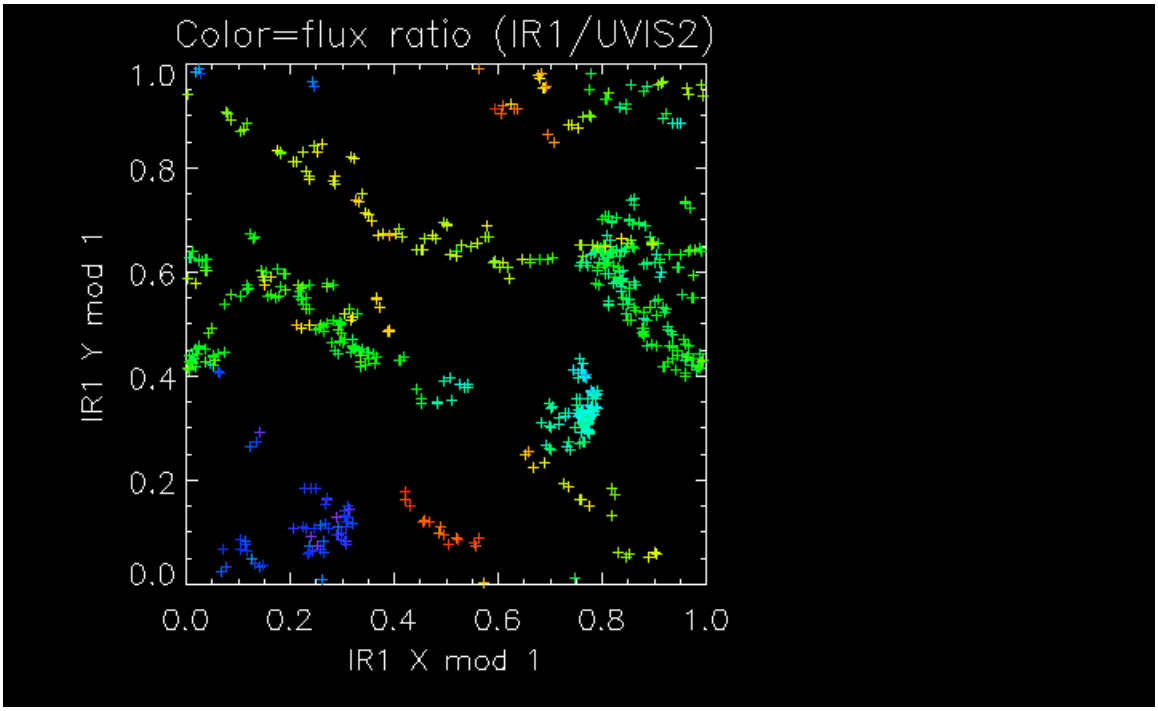

Figure 8: The ratio of integrated flux in a circular photometric aperture on IR-1 to that on UVIS-2, rendered in color on a representative pixel. The center, edges, and corners of the plot correspond to the center, edges, and corners of a representative WFC3 IR-1 pixel. The color scale corresponds linearly to ratios of 0.96 (purple) to 1.04 (red), after renormalization to the median ratio.

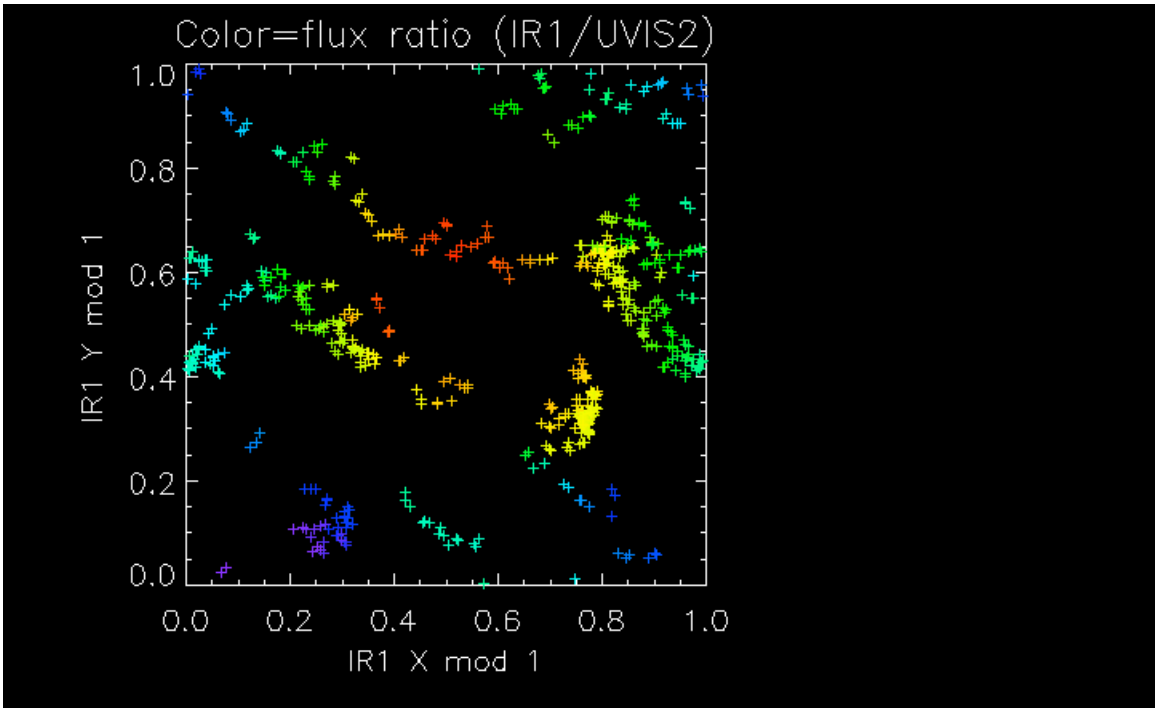

Figure 9: Same as Figure 8, except this diagram renders the flux ratio of only the brightest pixel of IR-1 to the integrated flux of UVIS-2, and the color scale, which corresponds linearly to ratios of 0.51 (purple) to 1.28 (red), after renormalization to the median ratio.